



Simple and rapid synthesis of magnetic kiwifruit for the removal of sitagliptin and fampridine residues from aqueous media using HPLC method: optimization via central composite experimental design

Faranak Aslanzadeh¹ · Elaheh Konozi¹ · Ali Niazi¹ · Alireza Feyz Bakhsh¹ · Ali Ezabadi¹

Received: 8 October 2022 / Accepted: 2 May 2023 / Published online: 18 May 2023
© Institute of Chemistry, Slovak Academy of Sciences 2023

Abstract

In this study, the magnetic biosorbent was synthesized from kiwi peel and applied to eliminate Sitagliptin (STG) and Fampridine (FMP) from aqueous media using high-performance liquid chromatography (HPLC). The maximum removal percentage was found to be 69.04% and 63.76% for STG and FMP, respectively. The characterization of adsorbent was evaluated using a scanning electron microscope (SEM), transmission electron microscopy (TEM), Fourier-transform infrared spectroscopy (FTIR), X-ray diffraction analysis (XRD), and vibrating-sample magnetometer (VSM). The optimization of variables, including pH, adsorbent dosage, and contact time, influencing the peak area were investigated via the central composite design (CCD). The highest peak area of the STG (actual: 2170.1, predicted: 2170.21) was obtained at a pH of 7.8, an adsorbent dosage of 15.5 mg, and a contact time of 35.5 min. Also, the maximum peak area of FMP (actual: 1932.5, predicted: 1901.11) was related to the pH = 7.8, adsorbent dosage of 11.8 mg, and contact time of 33.5 min. The significance and adequacy of the model and experimental variables were assessed using analysis of variance (ANOVA). The results indicated that the quadratic model is acceptable for the prediction of peak areas of STG and FMP. The magnetic kiwi peel as a simple and low-cost adsorbent with easy fabrication was found to be efficient for STG and FMP removal from the aqueous environments.

Keywords Kiwi peel · Magnetic · Pharmaceutical pollutants · High-performance liquid chromatography · Central composite design

Introduction

Water pollution is one of the most important issues around the world because clean water is essential for both life and economic development. In recent years, by increasing the activity of agricultural, industrial, and urban, the contamination level has been enhanced in the environment and especially in aquatic bodies. Dyes, pesticides, fertilizers, pharmaceuticals, organic material, nutrients, oils, and heavy metals are common contaminants (Castro et al. 2021). Wherever there are humans, drugs enter environments such as aqueous media, soil, and sediments because they can be resistant to degradation at wastewater treatment plants (WWTPs) (Mrozik and Stefanska, 2014). Also, part of the drugs enter

the wastewater stream after human consumption (Angeles et al. 2020). Low concentrations of drugs are dangerous to humans, animals, and aquatic organisms (Liakos et al. 2021).

One of the pharmaceutical contaminants is Sitagliptin (STG) (Fig. 1a), which was the first dipeptidyl peptidase-4 (DPP-4) inhibitor for treating diabetes mellitus (DM). By the inhibition of DPP-4 and increasing insulin secretion, a decrease of glucagon-like peptide-1 (GLP-1) breakdown occurs, which leads to a decrease in blood sugar level (Kit Loh et al. 2020; Gumieniczek et al. 2019). Some studies showed its chemical stability in stressed conditions such as high temperature, acidic and basic pH (Krakko et al. 2022). Owing to its high persistence and increasing consumption, it is discharged in significant quantities by wastewater treatment plants (WWTPs) with concentrations up to 1.0 µg/L in WWTP effluents (Hermes et al. 2020).

The other drug as contaminant in aqueous media is Fampridine (FMP) (Fig. 1b), which is prescribed to improve walking disorders in patients suffering from multiple sclerosis (MS) (Suneetha and Raja Rajeswari 2016; Achanti and

✉ Elaheh Konozi
konozelaheh@gmail.com

¹ Department of Chemistry, Faculty of Science, Central Tehran Branch, Islamic Azad University, Tehran, Iran

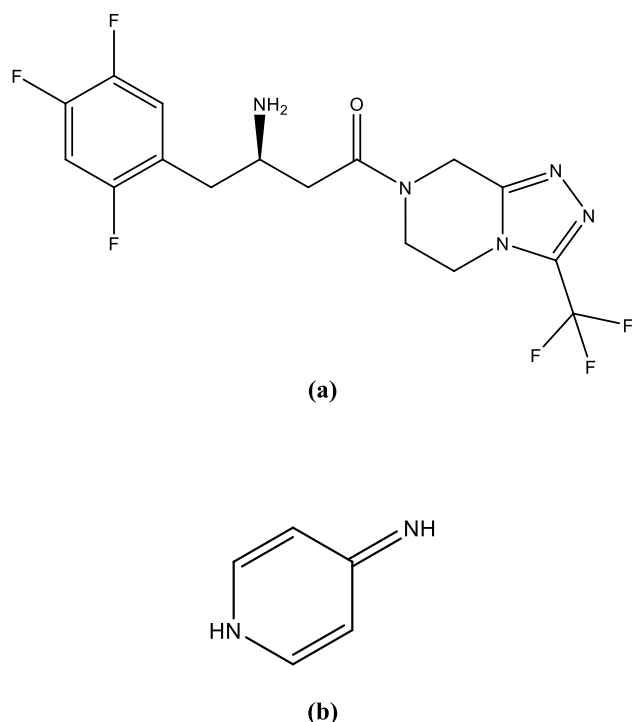


Fig. 1 Chemical structure of **a** STG and **b** FMP

Rajeswari Katta 2016). It is a selective potassium channel blocker, which increases the signal transfer in demyelinated nerve fibers. Therapy with prolonged-release (PR) FMP increases walking speed and stability, as well as it can create a better balance (Weller et al. 2020). The existence of this drug in the environment can lead to the degradation of surface and subsurface water quality, consequently impacting the health of living organisms. Also, its effects on aquatic populations can be observed (Bankole et al. 2023).

The presence of pharmaceuticals in aquatic environments for a long time has harmful effects on human health such as cancer, mutation, allergic reactions, and drug resistance (Mahmoud et al. 2020). Therefore, it is important to remove drugs from aqueous ecosystems.

Several procedures, including ozonation (Hermes et al. 2020), advanced oxidation (Almomani et al. 2016; Kanakaraju et al. 2018), coagulation (Gou et al. 2017), of coagulation/flocculation (Kooijman et al. 2020), nanofiltration (Gomes et al. 2020), ultrafiltration (Baresel et al. 2019), and adsorption (Dhiman et al., 2019) have been reported to eliminate types of drugs from aqueous solutions. Among the mentioned methods, adsorption is simple, affordable, high efficiency, and environmentally

friendly, which has been extensively used to remove contaminants (Abolhasani et al. 2019; Singh et al. 2017). Bioadsorbents possess some advantages such as inexpensive, easy access, high performance, good adsorption capacity, easy regeneration, and eco-friendly (Mallampati et al. 2015; Pathak et al. 2015). Lemon peel (Bhattacharyya et al. 2019), potato peels (Kyzasa and Deliyanni 2015), rice husk ash (Swarnalakshmi et al. 2018), tea waste (Patil et al. 2019), and others are various bioadsorbents, which have been used to eliminate pharmaceutical contaminants.

Kiwifruit belongs to the *Actinidia* genus which includes diverse species and cultivars with several combinations. This small meaty green fruit contains small black seeds, and a brown skin cover the fruit. Kiwi peel has mainly carbohydrates, as well as the minerals with the maximum value are Mg (8200 ppm), K (2300 ppm), Ca (2300 ppm), Na (900 ppm), P (600 ppm), Fe (82.26 ppm), Cu (6.64 ppm), Zn (9.26 ppm), and Mn (14.83 ppm). There is phenolic content along with chlorogenic acid, protocatechuic acid, p-hydroxybenzoic acid, caffeic acid, quercetin, and rutin in the kiwi peel (Sanz et al. 2021). Therefore, its peel has diverse functional groups, which may be applied as an adsorbent for the removal of drugs from aqueous media. Gubitosa et al., used Kiwi peels as an adsorbent for the removal of propranolol from water (Gubitosa et al. 2022a, b). In the other study, Kiwi peels were used as a long-lasting and recyclable adsorbent to eliminate emerging pollutants such as ciprofloxacin (Gubitosa et al. 2022a, b). Owing to its low specific gravity and trend to agglomerate, the separation of this bioadsorbent is an important problem. These are limitations for wide usage for the batch and column processes. A proper method is a magnetic separation that solid particles can be separated using an external magnetic field (Jiang et al. 2015). The most magnetic substance in nature is Fe_3O_4 , which is very beneficial in the adsorption approach (Akpomie and Conradie 2020). The magnetic feature makes it easy to separate the adsorbent through an external magnet (Abbaszadeh et al. 2017).

In this study, the magnetic kiwi peel was prepared as a new, simple, environmentally friendly, easy availability, and inexpensive (without using any sophisticated equipment) bioadsorbent for the removal of STG and FMP from aqueous solutions. This is the first paper to use the magnetic kiwi peel to evaluate the STG and FMP removal from aqueous solutions. The use of cheap materials and simple laboratory conditions in this synthesis makes it significant and affordable for mass production. The characterization

of this adsorbent was assessed by scanning electron microscope (SEM), transmission electron microscopy (TEM), Fourier-transform infrared spectroscopy (FTIR), X-ray diffraction analysis (XRD), and vibrating-sample magnetometer (VSM). Statistical optimization of empirical parameters, which are effective on the peak area values was surveyed with central composite design (CCD) as a subset of response surface methodology (RSM). Moreover, the isotherm (Langmuir and Freundlich) and kinetic models (pseudo-first-order, pseudo-second-order) were studied.

Experimental

Materials

STG and FMP with a purity of 99.4% were prepared from Stereokem and Procos companies, respectively. Potassium dihydrogen phosphate (KH_2PO_4), ammonium acetate ($\text{NH}_4\text{CH}_2\text{CO}_2$), and sodium 1-octanesulfonate ($\text{C}_8\text{H}_{17}\text{NaO}_3\text{S}$) were purchased from Merck.

Apparatus

The surface morphology of the magnetic kiwi peel was evaluated using Sigma VP-500 SEM (TSCAN company, Czech). In the SEM method, kiwi peel powder was fixed on a carbon layer. Then, a gold layer (with an amount of Angstrom) was placed on it, and the photo was taken. In order to determine the size of the adsorbent, TEM (Zeiss company, Germany, EM 10C–1000 kV) was applied. FTIR (PerkinElmer, U.S.A) at a wavenumber range from 4000 to 400 cm^{-1} was used to study the functional groups of the adsorbent. The XRD (Malvern Panalytical company, United Kingdom) was utilized to record the XRD pattern of Fe_3O_4 and magnetic kiwi peel at the 2θ range from 10° to 80° .

Preparation of magnetic adsorbent

6.1 g iron(III) chloride hexahydrate ($\text{FeCl}_3 \cdot 6\text{H}_2\text{O}$) and 4.2 g iron(II) sulfate were dissolved in 100 mL of distilled

water. This solution was transferred to a round-bottom flask and its temperature increased to 90°C using a heater stirrer. Then, 1 g of kiwi peel powder was dispersed in 200 mL distilled water. Afterward, 10 mL NaOH (0.5 M) and dispersed kiwi peel were poured into the round-bottom flask, respectively. Using NaOH (0.5 M), the pH was set to 10 and exposed to a temperature of 80°C for 30 min. After cooling, it was transferred to a beaker and the precipitate was collected using a magnet, as well as the supernatant was discarded. The precipitate was dried in an oven at 40°C for 24 h and was powdered in a mortar.

Standard solution preparation

1000 mL solution of STG and FMP with concentration of $30\text{ }\mu\text{g mL}^{-1}$ was prepared separately (stock solutions). Then, the standard solutions with concentrations of 25, 20, 15, 10, and $5\text{ }\mu\text{g mL}^{-1}$ were individually prepared from stock solutions. 5 mg of adsorbent was added to one of the parts. The solutions were injected into the HPLC instrument for plotting calibration curve.

Preparation of real sample

STG and FMP products were produced in the form of tablets at Alhavi Pharmaceutical Company. After cleaning and washing the production line, sampling of rinse water obtained from washing was done at 3 points. Then, drug removal was done by magnetic NPs.

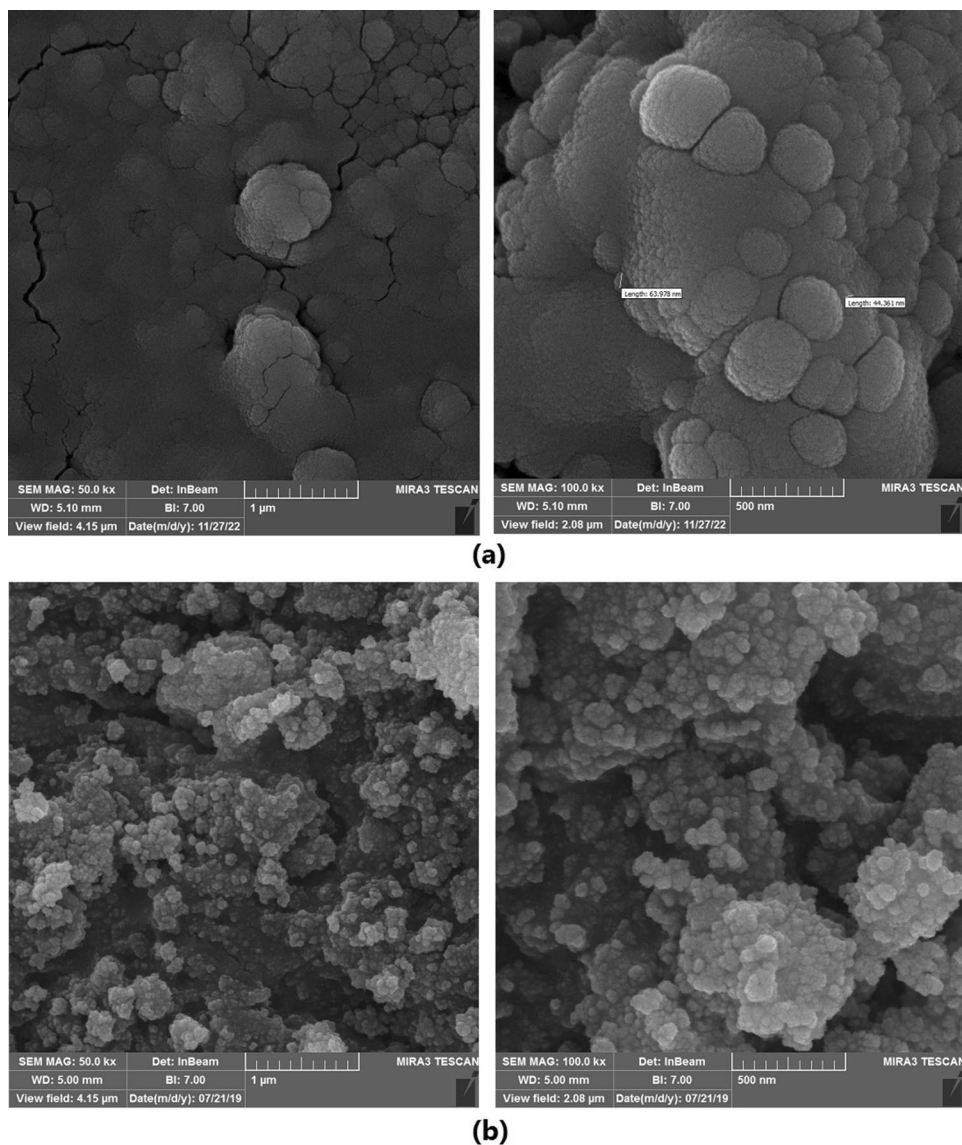
Chromatographic conditions

Chromatographic analysis was accomplished with an HPLC system (Agilent 1200 series) with a C18 column ($25\text{ cm} \times 4.6\text{ mm}$, $5\text{ }\mu\text{m}$). The mobile phase related to the STG and FMP was phosphate buffer, methanol, acetonitrile (60:30:10 v/v/v) and phosphate buffer, methanol (70:30 v/v), respectively. The mobile phase flow rate was adjusted to 1 ml/min for both components with the injection volume of 20 μL . The STG and FMP wavelength was set at 268 and 240 nm, respectively.

Table 1 The levels of pH, adsorbent dosage, and time in CCD model for STG and FMP

Factor	STG					FMP	
	α	-1	0	+1	$+\alpha$	Low level	High level
A (pH)	5.60	6.50	7.80	9.00	9.90	6.5	9
B (Adsorbent dosage (mg))	8.00	9.50	11.8	14.0	15.5	9.5	14
C (Time (min))	14.2	22.0	33.5	45.0	52.8	22	45

Fig. 2 SEM image of **a** powder kiwi peel before adding Fe_3O_4 and **b** magnetic kiwi peel



Removal experiments

The removal of STG and FMP was assessed by magnetic kiwi peel, and estimation of removal percentage was accomplished at various concentrations of pollutant (1–1500 $\mu\text{g}/\text{mL}$) with a volume of 25 mL, time between 1 and 45 min, different peak areas, the adsorbent dosage of 15 mg and pH of 9.

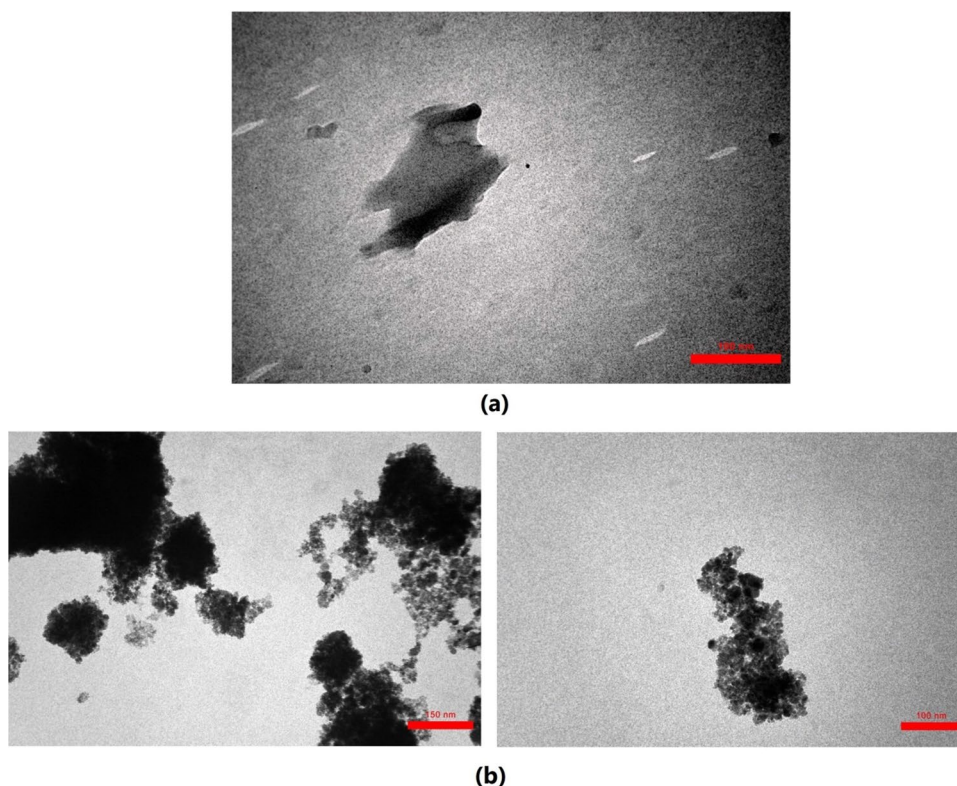
Central composite design (CCD)

A single-factor experimental design is commonly performed by researchers, which is named as one-factor-at-a-time (OFAT) method. In this approach, only one variable

is changed at a time and the other variables are constant. The experimental ranges can be obtained for each parameter without eliminating any conditions, which is the advantage of the OFAT method. However, this technique is time-consuming and it does not represent the interaction effects among the factors, which makes it difficult to achieve optimal safety conditions. Therefore, RSM can be proposed as a statistical method (Amirah Mohd Zahri et al. 2021). The CCD is a powerful form of RSM, which investigates the factors affecting the experiment (Rao Amarachinta et al. 2021). The benefit of this approach is time-saving through screening of more factors (Elshafei et al. 2021).

In this study, the interaction between pH, contact time, and nano dosage was assessed using CCD and 17 experiments were obtained using Eq. (1).

Fig. 3 TEM image of **a** powder kiwi peel before adding Fe_3O_4 and **b** magnetic kiwi peel



$$N = 2^n + 2n + n_c \quad (1)$$

where n and n_c denote the number of independent factors and number of center points. Also, the total of experiments is shown by N (Bayuo et al., 2020). The factor levels of STG and FMP are given in Table 1. The predicted values were determined using a quadratic model as represented in Eq. (2).

$$Y = \beta_0 + \sum_{i=1}^k \beta_i X_i + \sum_{i=1}^k \beta_{ii} X_i^2 + \sum_{i=1}^k \sum_{i \neq j=1}^k \beta_{ij} X_i X_j + \varepsilon \quad (2)$$

where Y demonstrates the response value. β_0 , β_i , β_{ii} , and β_{ij} depict the constant coefficient, linear, quadratic, and interaction effects, respectively. The independent variables are shown by X_i and X_j , as well as ε and k indicate the error and the number of factors, respectively (Farhadi et al. 2021).

Results and discussion

Characterization

SEM analysis

SEM image of powder kiwi peel (Fig. 2a) displays spherical shape. Figure 2b reveals the SEM image of the kiwi

peel after modification with Fe_3O_4 . The magnetic Fe_3O_4 is dispersed on the peel surface and the agglomerated morphology with a spherical structure is observed. This image signifies the homogeneous distribution of spherical nanoparticles.

TEM analysis

The TEM image of kiwi peel before adding Fe_3O_4 is exhibited in Fig. 3a. No specific agglomeration is observed. On the other hand, the prepared magnetic kiwi peel has an agglomerated spherical morphology, which indicated that Fe_3O_4 particles are located on the peel surface (Fig. 3b). The aggregation of NPs is due to their superparamagnetic nature.

FTIR analysis

The FTIR spectrum of kiwi peel is shown in Fig. 4a. The band at 3444 cm^{-1} corresponds to hydroxyl group. The absorption peak at 2917 cm^{-1} indicates the functional group C–H. The peak at 1733 cm^{-1} is stretching vibration of carboxyl (COOH) group. The peaks at 1247 cm^{-1} and 1045 cm^{-1} are assigned to the C–C and C–H bending, respectively (Sartape et al. 2017). As illustrated in Fig. 4, the broad peak at 3424 cm^{-1} is related to the hydroxyl groups on the magnetic adsorbent surface. The peak at

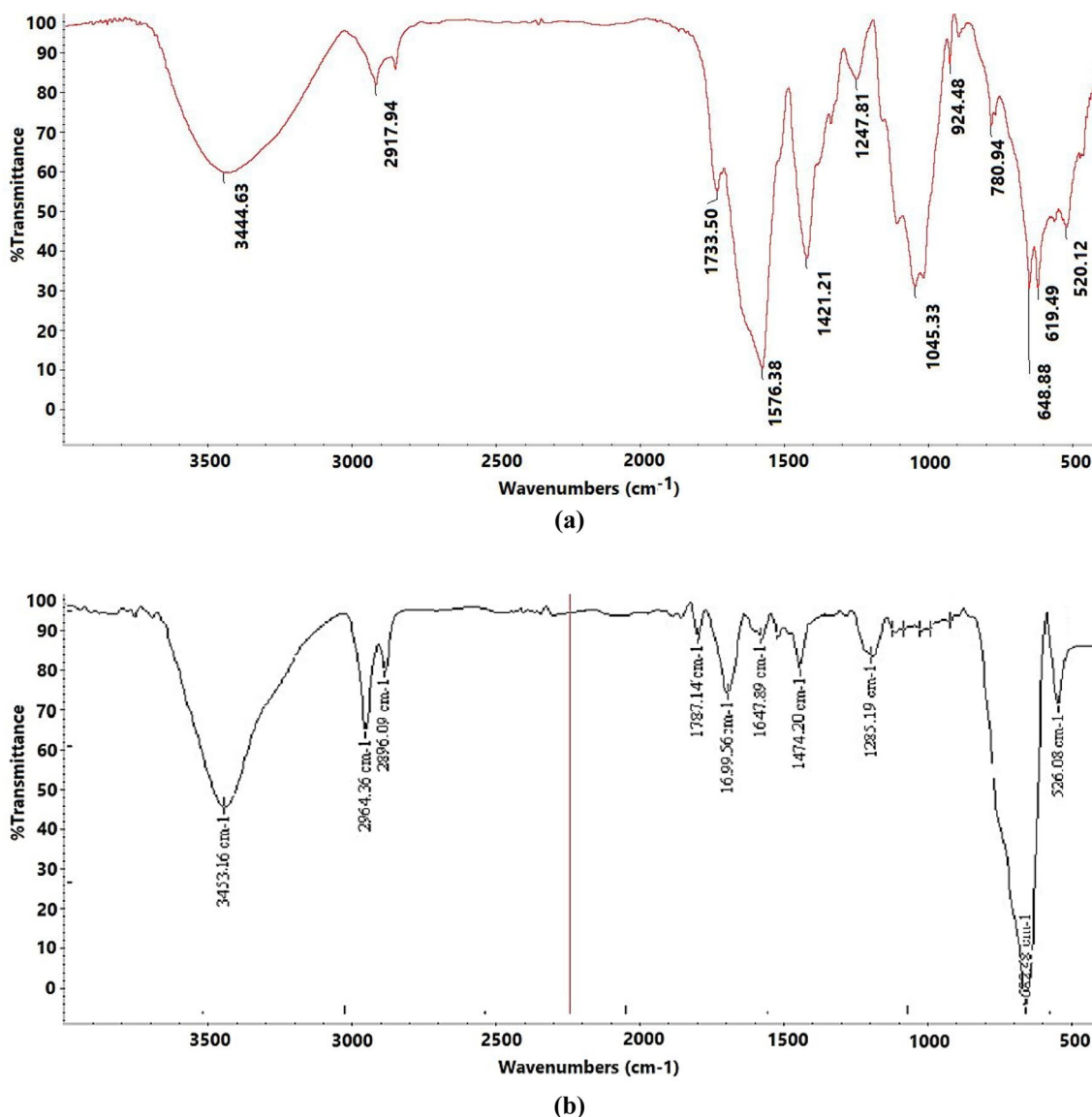


Fig. 4 FTIR spectrum of **a** kiwi peel powder before adding Fe₃O₄ and **b** magnetic kiwi peel

2923 cm⁻¹ represents the stretching vibration of the C–H (Jiang et al. 2015; Weng et al. 2018). The absorption band at 2899 cm⁻¹ confirms the existence of the –CH₂ group (Singh et al. 2017). The peak at 1747 cm⁻¹ belongs to the stretching vibration of C=O of ester or carboxylic acid functional groups (Mallampati et al. 2015). The absorption peak at 1639 cm⁻¹ shows the stretching vibration of C=O for carboxylic groups. The observed peak at 1384 cm⁻¹ is attributed to –CH₃, which is specific. The sharp peak at 582 cm⁻¹ is due to the presence of the Fe–O–Fe bond of Fe₃O₄ (Abbaszadeh et al. 2017; Pashazadeh-Panahi and Hasanzadeh 2020).

XRD analysis

The observed peaks at $2\theta = 29.89^\circ, 35.36^\circ, 43.19^\circ, 53.43^\circ, 57.14^\circ,$ and 62.82° (Fig. 5a) are assigned to the (220), (311), (400), (422), (511), and (440) planes. These peaks are similar to the peaks in the standard pattern of magnetite Fe₃O₄ (JCPDS 19–0629) (Chang Lin and Yen Lee 2020; Liu et al. 2020). The XRD spectra of kiwi peel before adding Fe₃O₄ (Fig. 5b) showed a sharp peak at 2θ value around 25° . In Fig. 5c, a similar pattern of Fe₃O₄ can be observed, where

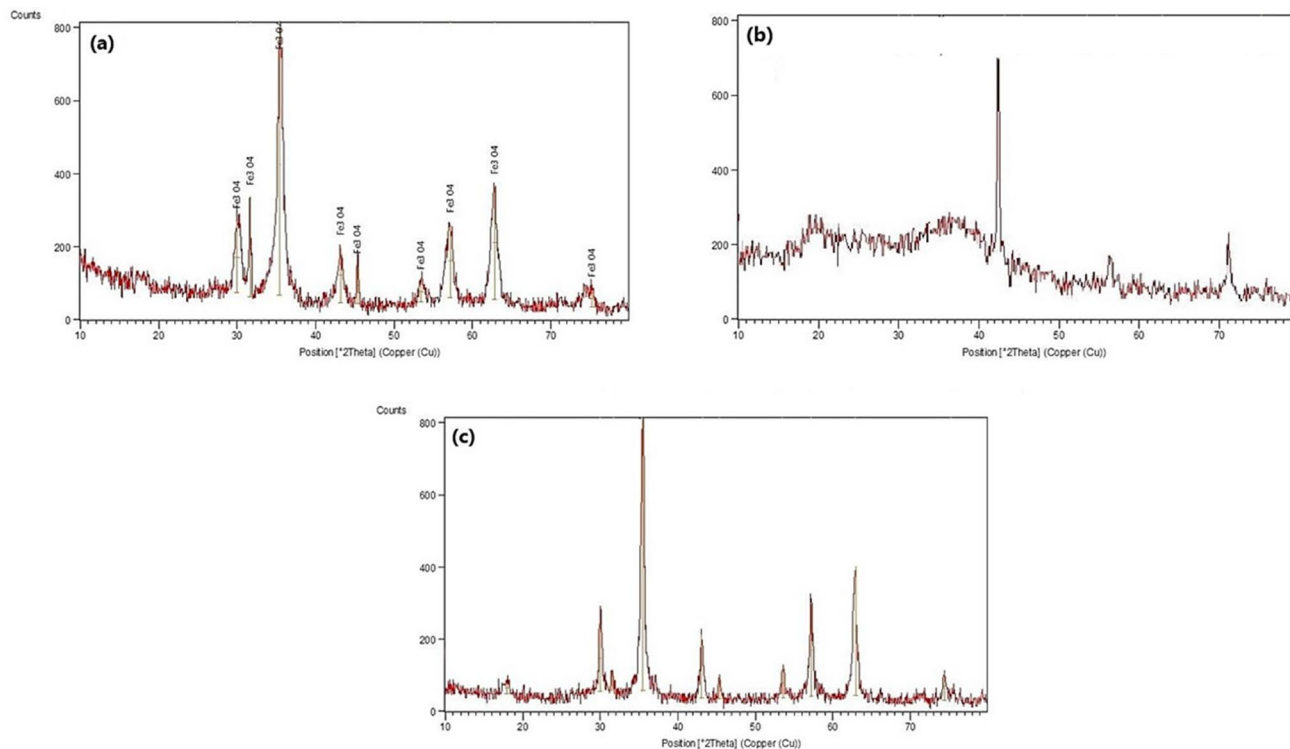
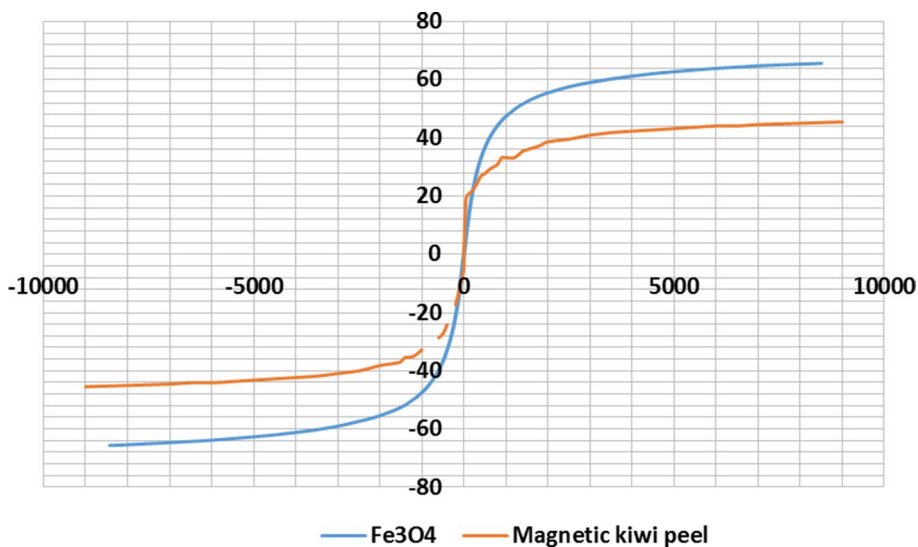


Fig. 5 XRD pattern of **a** Fe_3O_4 , **b** kiwi peel before adding Fe_3O_4 , and **c** magnetic kiwi peel

Fig. 6 VSM analysis of Fe_3O_4 and magnetic kiwi peel



the crystallinity corresponding to the magnetic kiwi peel remained the same. It can be stated that the formation of this adsorbent does not indicate any effect on the magnetic property of Fe_3O_4 .

VSM analysis

The magnetic feature of Fe_3O_4 and magnetic kiwi peel was assessed by VSM (Fig. 6). The magnetization of Fe_3O_4 and

magnetic kiwi peel was found to be 65.58 and 45.45 emu/g, respectively. These results reveal that the kiwi peel was successfully magnetized by coating with Fe_3O_4 NPs. The decline in the magnetization of the kiwi peel may be assigned to the decreased ferrite content in the kiwi peel and the formation of an outer layer of metal oxides over the surface of the Fe_3O_4 core.

Table 2 The obtained removal percentage related to the STG and FMP

Conc ($\mu\text{g/mL}$)	Area		Remain		Removal (%)	
	STG	FMP	STG	FMP	STG	FMP
1	164.93	1750.16	30.95	36.98	69.04	63.01
5	194.41	1749.91	36.48	36.97	63.51	63.02
10	194.39	1750.17	36.48	36.98	63.51	63.01
50	214.68	1714.85	40.29	36.23	59.70	63.76
100	379.41	1751.01	71.20	36.99	28.79	63.00
250	391.72	1791.21	73.51	37.84	26.48	62.15
500	415.86	1725.63	78.04	36.46	21.95	63.53
1000	415.72	1765.16	78.02	37.29	21.97	62.70
1500	416.14	1732.75	78.09	36.61	21.90	63.38

Table 3 CCD results and interaction between factors related to the STG

Run	pH	Nano dosage (mg)	Time (min)	Actual	Predicted
1	6.5	14.0	22.0	1860.0	1860.17
2	7.8	11.8	33.5	1951.3	1951.31
3	7.8	11.8	14.2	1705.9	1705.93
4	5.6	11.8	33.5	1840.0	1840.01
5	9.0	14.0	45.0	1992.3	1992.36
6	6.5	9.50	45.0	2032.9	2032.88
7	7.8	8.00	33.5	1935.2	1935.22
8	7.8	11.8	52.8	1849.5	1849.48
9	6.5	9.50	22.0	2061.5	2061.51
10	7.8	11.8	33.5	1940.5	1940.47
11	9.0	9.50	45.0	1552.3	1552.35
12	7.8	11.8	33.5	1932.8	1932.81
13	9.9	11.8	33.5	1301.5	1301.46
14	7.8	15.5	33.5	2170.1	2170.21
15	9.0	9.50	22.0	1400.0	1399.96
16	6.5	14.0	45.0	1917.2	1916.98
17	9.0	14.0	22.0	1683.3	1682.99

Table 4 CCD results and interaction between factors related to the FMP

Run	pH	Nano dosage (mg)	Time (min)	Actual	Predicted
1	7.8	8.00	33.5	1861.9	1872.1
2	6.5	14.0	45.0	1669.9	1678.7
3	7.8	11.8	33.5	1891.0	1901.1
4	7.8	11.8	52.8	1697.1	1680.6
5	9.0	9.50	22.0	1752.0	1738.4
6	5.6	11.8	33.5	1620.0	1610.1
7	6.5	14.0	22.0	1685.3	1699.0
8	9.0	14.0	22.0	1722.7	1706.0
9	9.0	9.50	45.0	1715.7	1718.0
10	7.8	11.8	33.5	1932.5	1901.1
11	9.9	11.8	33.5	1621.0	1621.1
12	6.5	9.50	45.0	1721.0	1711.0
13	7.8	11.8	33.5	1878.3	1901.1
14	6.5	9.50	22.0	1722.4	1731.4
15	9.0	14.0	45.0	1654.0	1685.6
16	7.8	11.8	14.2	1707.4	1714.8
17	7.8	15.5	33.5	1837.0	1817.7

Removal results

The removal percentage of STG and FMP was calculated (Table 2). As shown, the maximum removal of STG (69.04%) was assigned to the concentration of 1 mg/mL and a peak area of 164.93. By increasing the concentration of STG from 1 to 1500 $\mu\text{g/mL}$, the removal percentage using the adsorbent was decreased. The diminish in the removal efficiency can be assigned to the less active sites in high concentrations, which prevent the drug from binding completely to the adsorbent surface (Rani and Shanker 2018). Also, the FMP concentration of 50 mg/mL with the peak area of 1714.85 represented the maximum removal percentage (63.76%). At lower concentrations of FMP up to 50 $\mu\text{g/mL}$, the specific surface area and abundant reactive surface center are high, which are more available to the target molecules. On the other hand, a decrease in the mass transfer occurs at concentrations higher than 50 $\mu\text{g/mL}$. Hence, there is a lack of available unoccupied sites of adsorbent.

Results of CCD

The implementation of the CCD approach was performed to evaluate the effect of pH, nano dosage, and time on the peak area value of STG and FMP (Table 3 and Table 4). As shown in these tables, the actual and predicted peak area values were compared with each other. The maximum peak area of the STG (actual = 2170.1, predicted = 2170.21) was assigned to the pH = 7.8, nano adsorbent of 15.5 (mg), and contact time of 33.5 min. On the other hand, the highest peak area of FMP (actual = 1932.5, predicted = 1901.11) was related to the obtained values at the pH = 7.8, nano adsorbent of 11.8 (mg), and contact time of 33.5 min. In order to determine peak area, a quadratic equation was applied for STG and FMP using Eqs. 3 and 4, respectively.

Table 5 ANOVA results of CCD for the prediction of peak area of STG

Source	Sum of squares	df	Mean square	F-value	P-value	Prob > F
Model	8.605E+005	9	95,606.9	287.46	<0.0001	Significant
A-pH	3.357E+005	1	3.357E+005	1009.4	<0.0001	–
B-nano	46,573.7	1	46,573.7	140.03	<0.0001	–
C-time	34,717.1	1	34,717.1	104.38	<0.0001	–
AB	1.291E+005	1	1.291E+005	388.11	<0.0001	–
AC	26,007.4	1	26,007.4	78.200	<0.0001	–
BC	8903.49	1	8903.49	26.770	0.0013	–
A ²	1.919E+005	1	1.919E+005	577.05	<0.0001	–
B ²	19,503.8	1	19,503.8	58.640	0.0001	–
C ²	35,526.5	1	35,526.5	106.82	<0.0001	–
Residual	2328.15	7	332.590	–	–	–
Lack of fit	2155.43	5	431.090	–	–	Not significant
Pure error	172.730	2	86.3600	4.9900	0.1753	–
Cor total	8.628E+005	16	–	–	–	–
R-Squared	0.9973					
Adj R-Squared	0.9938					
Pred R-Squared	0.9803					

Table 6 ANOVA results of CCD for the prediction of peak area of FMP

Source	Sum of squares	df	Mean square	F-value	P-value	Prob > F
Model	1.466E+005	6	24,432.3	55.17	<0.0001	Significant
A-pH	165.080	1	165.080	0.37	0.5551	–
B-nano	3578.78	1	3578.78	8.080	0.0175	–
C-time	1417.24	1	1417.24	3.200	0.1039	–
A ²	1.146E+005	1	1.146E+005	258.6	<0.0001	–
B ²	4444.91	1	4444.91	10.04	0.0100	–
C ²	58,278.5	1	58,278.5	131.6	<0.0001	–
Residual	4428.16	10	442.820	–	–	–
Lack of fit	2821.10	8	352.640	0.4400	0.8353	Not significant
Pure error	1607.06	2	803.530	–	–	–
Cor total	1.510E+005	16	–	–	–	–
R-Squared	0.9707					
Adj R-Squared	0.9531					
Pred R-Squared	0.9118					

$$R1 = 1946.07155.32 A + 58.63 B + 50.48 C \\ + 126.97 AB + 57.00 AC + 33.36 BC + 125.88 A^2 \\ + 42.31 B^2 + 56.42 C^2 \quad (3)$$

$$R1 = 1901.11 + 3.48A + 16.19 B + 10.19 C + 100.80 A^2 + 19.86 B^2 + 71.90C^2 \quad (4)$$

where A is the pH, B is the nano dosage (mg), and C is the time (min).

Statistical analysis

Analysis of variance (ANOVA) results related to the STG and FMP are given in Table 5 and Table 6. The results revealed the significance of the model where their F-value and P-value are 287.46 = STG, 55.17 = FMP and <0.0001, respectively. Furthermore, the “Prob > F” value is less than

0.05 indicating the significance of the model terms. Based on the p-values of STG ($p < 0.05$), all the linear coefficients, interaction coefficients, and quadratic coefficients were significant. On the other hand, the values higher than 0.05 show the insignificance of model terms. In the current case, the nano dosage (B) is significant model terms. “Adeq Precision” is known as one parameter to study signal-to-noise ratio. This value is proper where the ratio is higher than 4. In current models, the ratio values of STG and FMP were found to be 60.817 and 21.548, respectively, which represent the signal sufficiency and the model dependency. The high values of R^2 (STG = 0.9973, FMP = 0.9707) were obtained for the prediction of peak area under various conditions. In addition, the closeness adjusted R^2 value (STG = 0.9938, FMP = 0.9531) to the value of R^2 indicates the predicted values are near to the actual (experimental) values using the proposed model.

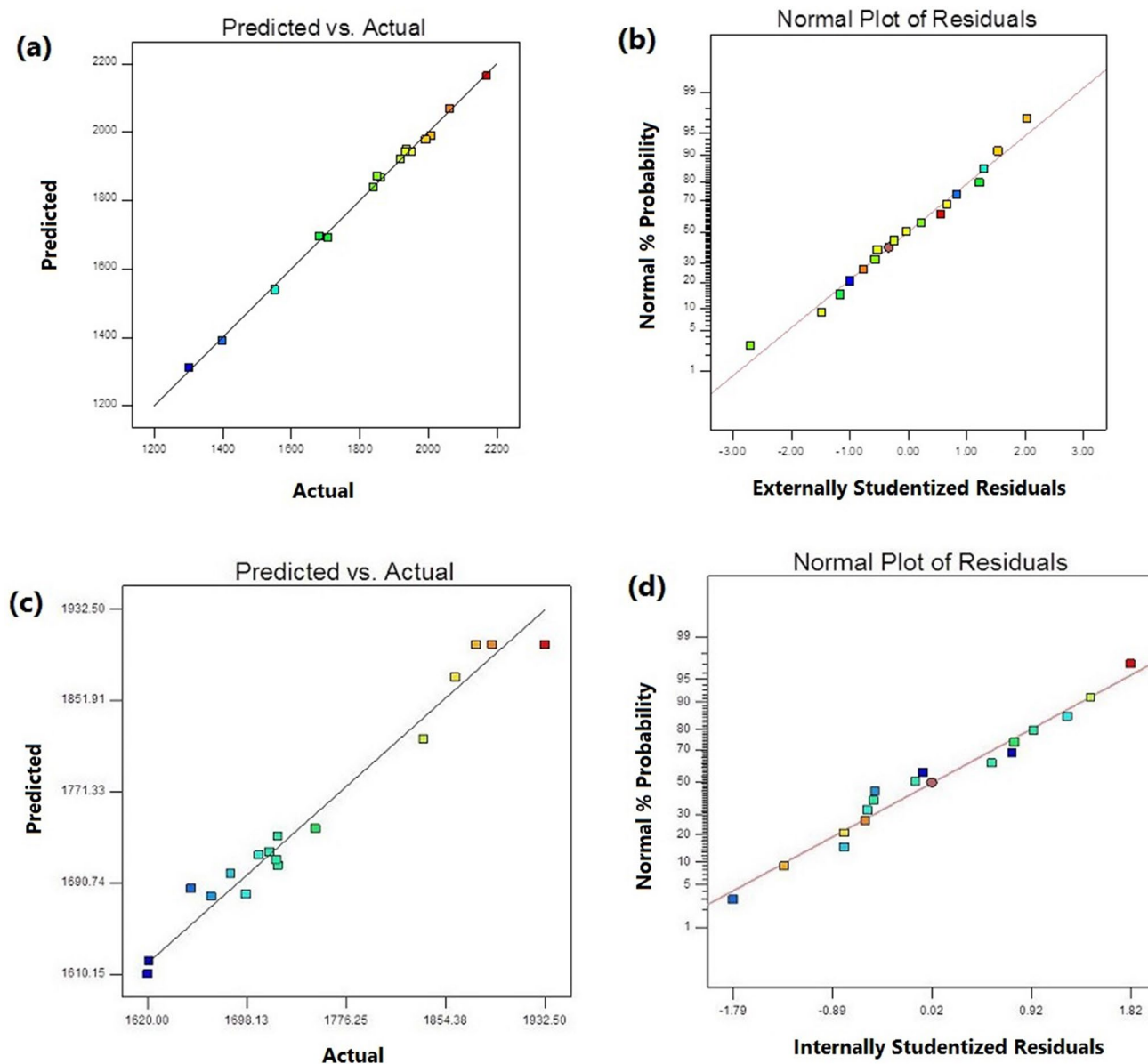


Fig. 7 Plot of predicted values versus actual values for **a** STG and **c** FMT, as well as a normal plot of residuals for **b** STG and **d** FMT related to the peak area values

The experimental values (actual) and CCD predicted values of STG were compared with each other (Fig. 7a). This plot represented that the values are very near to each other. Hence, the experiments possess excellent accuracy and less error. The normality of data was studied by a normal probability plot (Fig. 7b), indicating data points are located either on a straight line or in close proximity to the straight line. This propagation of data points confirms that the data have a normal distribution.

The obtained peak area values versus experimental values of the FMP are shown in Fig. 7c. The data is almost scattered around the straight line. These results suggest

that the two data sets have a high correlation with each other ($R^2 = 0.9707$). The diagram of the normal probability (%) against studentized residuals is exhibited in Fig. 7d. As shown, data possess a linear normal distribution without a certain variance.

3D response surface plots

In order to better visualize and quickly select optimal conditions, surface plots were used. The plots of STG and FMP are exhibited in Figs. 8 and 9, in which the optimum conditions, the relationships between parameters, and their mutual

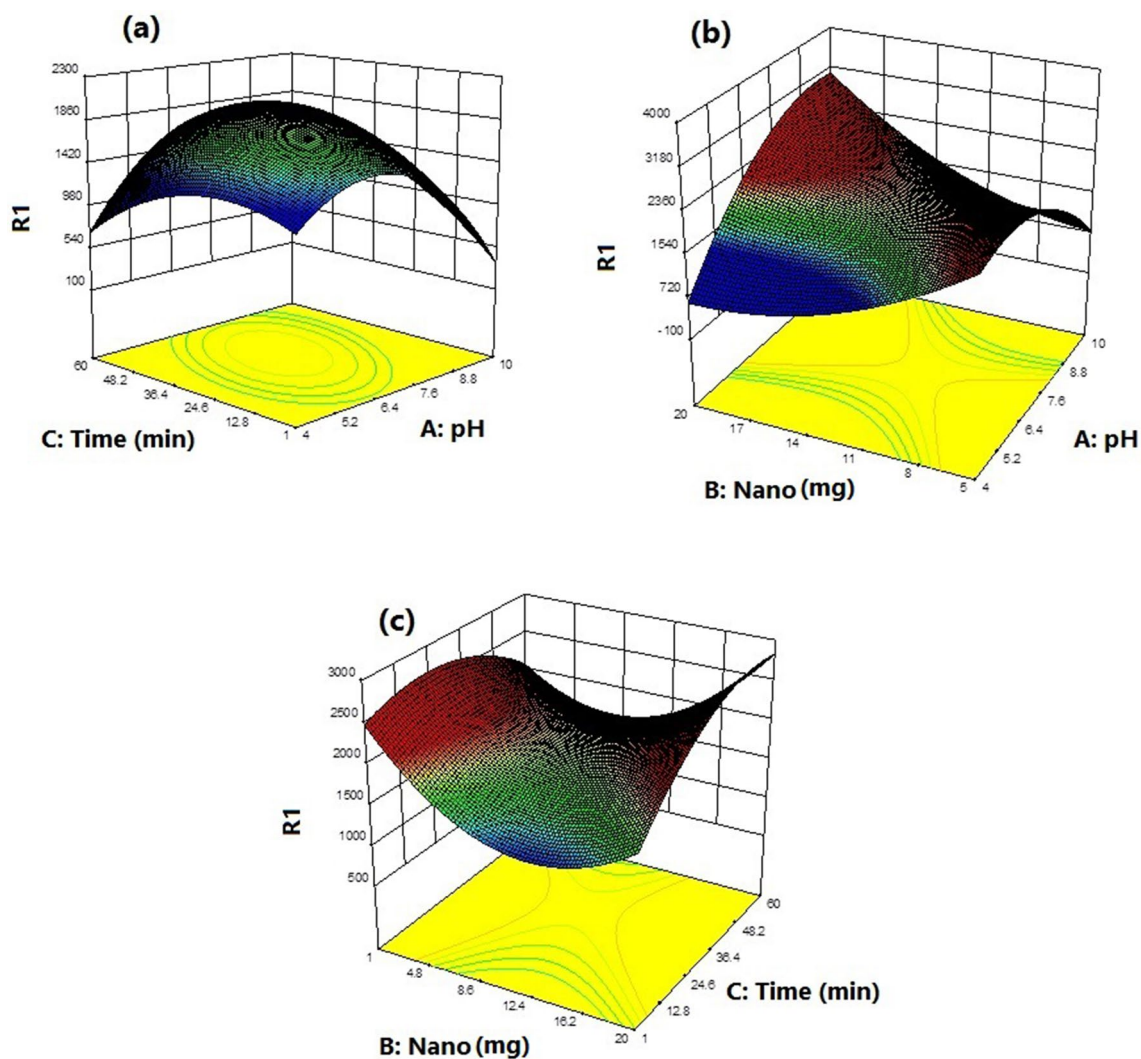


Fig. 8 3D response surface plots of CCD for the prediction of peak area related to the STG

dependence can be obviously assessed. The concurrent effect of two variables of time and pH on the peak area is displayed in the 3D diagram of Fig. 8a. The maximum peak area (1860) is proper at a pH value equal to 7.8 owing to the elevated electrostatic attraction force between the adsorbent and STG, because the increment of pH leads the adsorbent surface to become more negative. On the other hand, the decline of peak area with reducing pH can be attributed to the competition between STG ions and hydrogen ions for the active sites of the adsorbent (Kalantary et al. 2016).

The simultaneous effect of adsorbent dosage and pH on the peak area is shown in Fig. 8b. By increasing adsorbent dosage up to 15.5, the active sites and the surface areas available for the STG enhance.

According to Fig. 8c, the highest peak area is observed at 33.5 min, which is a sufficient opportunity for interaction between the adsorbent and STG. In fact, access to active sites of the adsorbent is more. The peak area value was increased up to 33.5 min. It can be concluded that at initial times all active sites related to the adsorbent surface are available. By decreasing available sites, the system was reached an equilibrium state.

Figure 9a illustrates the 3D surface plot related to the combined effects of pH (A) and time (C) on the peak area. The peak area was enhanced (1901.11) by increasing pH value and contact time up to 7.8 and 33.5 min, respectively. The mutual effect of the nano dosage (B) and pH (A) is represented in Fig. 9b. The highest peak area was

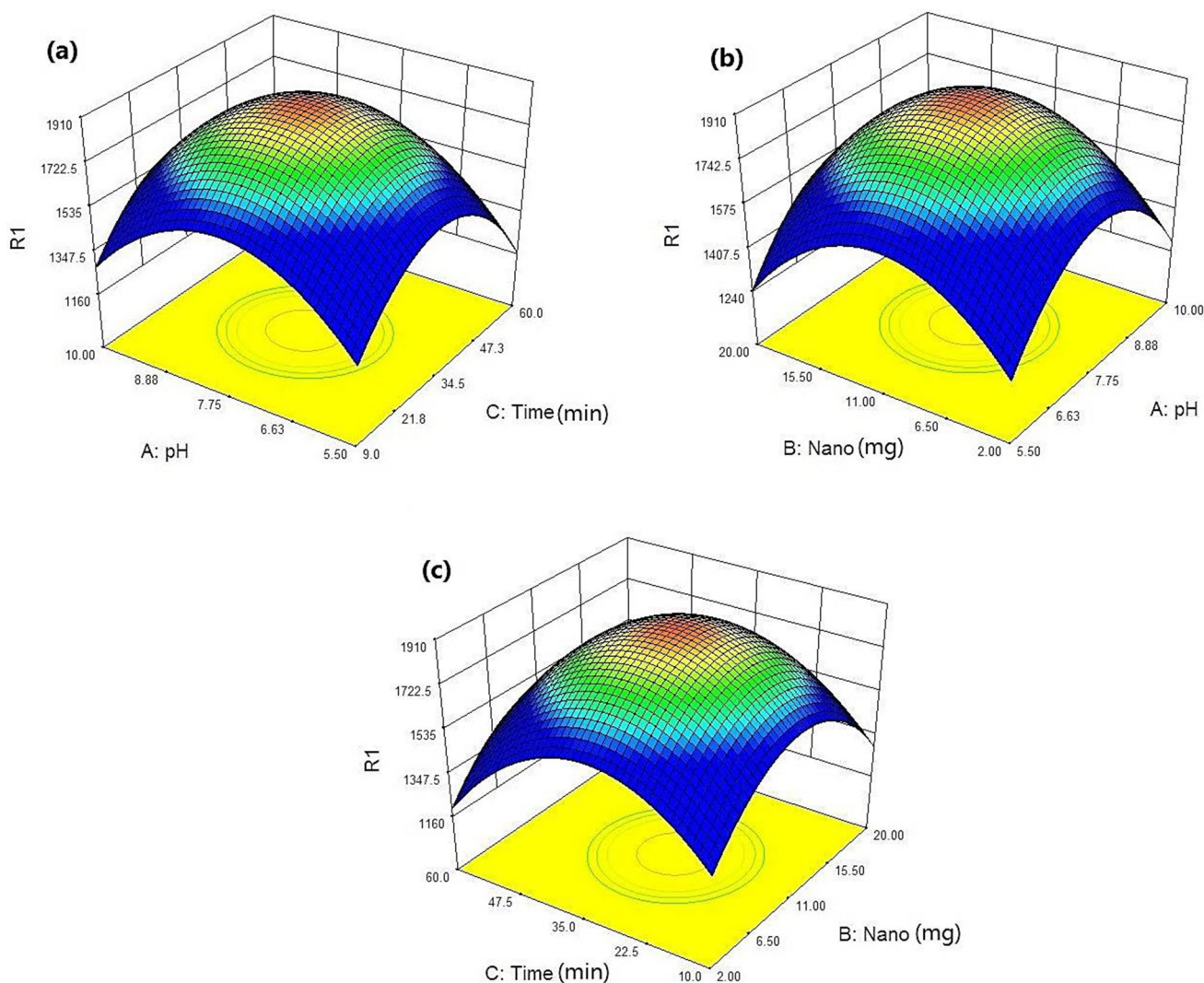


Fig. 9 3D response surface plots of CCD for the prediction of peak area related to the FMP

obtained by increasing the nano dosage up to 11.8 mg. At higher values of both parameters, the peak area was decreased. Moreover, it was discovered that by enhancing the time (up to 33.5 min) and nano dosage (up to 11.8), the response was improved (Fig. 9c).

Kinetic study

The kinetic data express the mechanism of transport rate related to the adsorbate onto the magnetic adsorbent. Two kinetic models, including pseudo-first-order (PFO) and pseudo-second-order (PSO) models were applied. The linear form PFO and PSO models are defined using Eqs. (5) and (6).

$$\ln(q_e - q_t) = \ln q_e - k_1(t) \quad (5)$$

$$\frac{t}{q_t} = \frac{1}{k_2 q_e^2} + \frac{t}{q_e} \quad (6)$$

In these equations, the amount of STG and FMP adsorbed at a certain time and equilibrium time is represented by q_t and q_e (mg g^{-1}), respectively. Also, K_1 (min^{-1}) and K_2 ($\text{g mg}^{-1} \text{min}^{-1}$) show the PFO and PSO rate constant, respectively. As shown in Fig. 10a, by plotting $\ln(q_e - q_t)$ versus t , the values of q_e and K_1 can be achieved from the slope and intercept, respectively (Table 7). The calculation of q_e and K_2 values of PSO (Table 7) was performed using the slope and intercept of the plot of t/q_t versus t , respectively

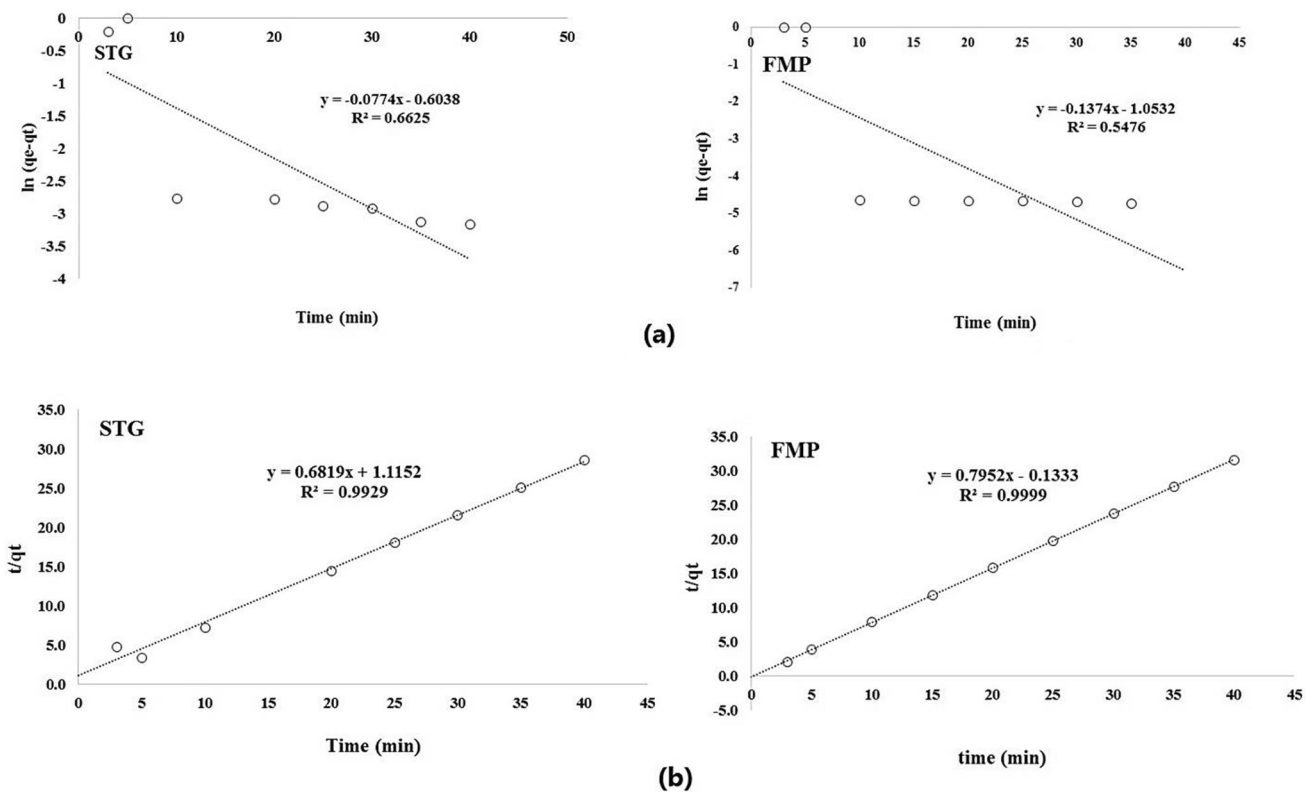


Fig. 10 **a** Pseudo first-order and **b** Pseudo second-order adsorption kinetics of STG and FMP by the magnetic kiwi peel

Table 7 The obtained kinetic parameters for the removal of STG and FMP

Kinetic	Parameters	STG	FMP
Pseudo-first-order	K_1 (min^{-1})	0.077	0.137
	q_e (mg g^{-1})	0.547	2.86
	R^2	0.662	0.547
Pseudo-second-order	K_2 ($\text{g mg}^{-1} \cdot \text{min}^{-1}$)	0.416	-4.74
	q_e (mg g^{-1})	1.46	1.25
	R^2	0.992	0.999

Table 8 The obtained parameters of isotherm models for the removal of STG and FMP

Kinetic	Parameters	STG	FMP
Langmuir	q_{max} (mg g^{-1})	59.88	58.08
	K_L (L/mg)	0.0250	0.1490
	R^2	0.9878	0.9667
Freundlich	K_f (mg g^{-1})	5.218	4.768
	$1/n$	0.3745	0.5263
	R^2	0.9144	0.7801

(Fig. 10b) (Radoor et al., 2021). The high R^2 (0.9999) of the PSO kinetic model reveals the goodness of fit of this model for the adsorption of both drugs. Hence, the control the reaction mechanism and adsorption rate of the PSO model are performed using the chemical adsorption.

Adsorption isotherm models

Adsorption isotherm studies indicate the interaction between the adsorbent and adsorbate. In this study, the interaction between adsorbent and STG and FMP was evaluated through Langmuir and Freundlich isotherm models that their assumption is monolayer and multilayer adsorption, respectively. The linear form of Langmuir and Freundlich isotherm models can be described using Eqs. (7) and (8), respectively.

$$\frac{C_e}{q_e} = \frac{1}{q_{\text{max}}K_L} + \frac{1}{q_{\text{max}}}C_e \tag{7}$$

$$\text{Log}q_e = \text{log}(K_F) + \frac{1}{n}\text{log}(C_e) \tag{8}$$

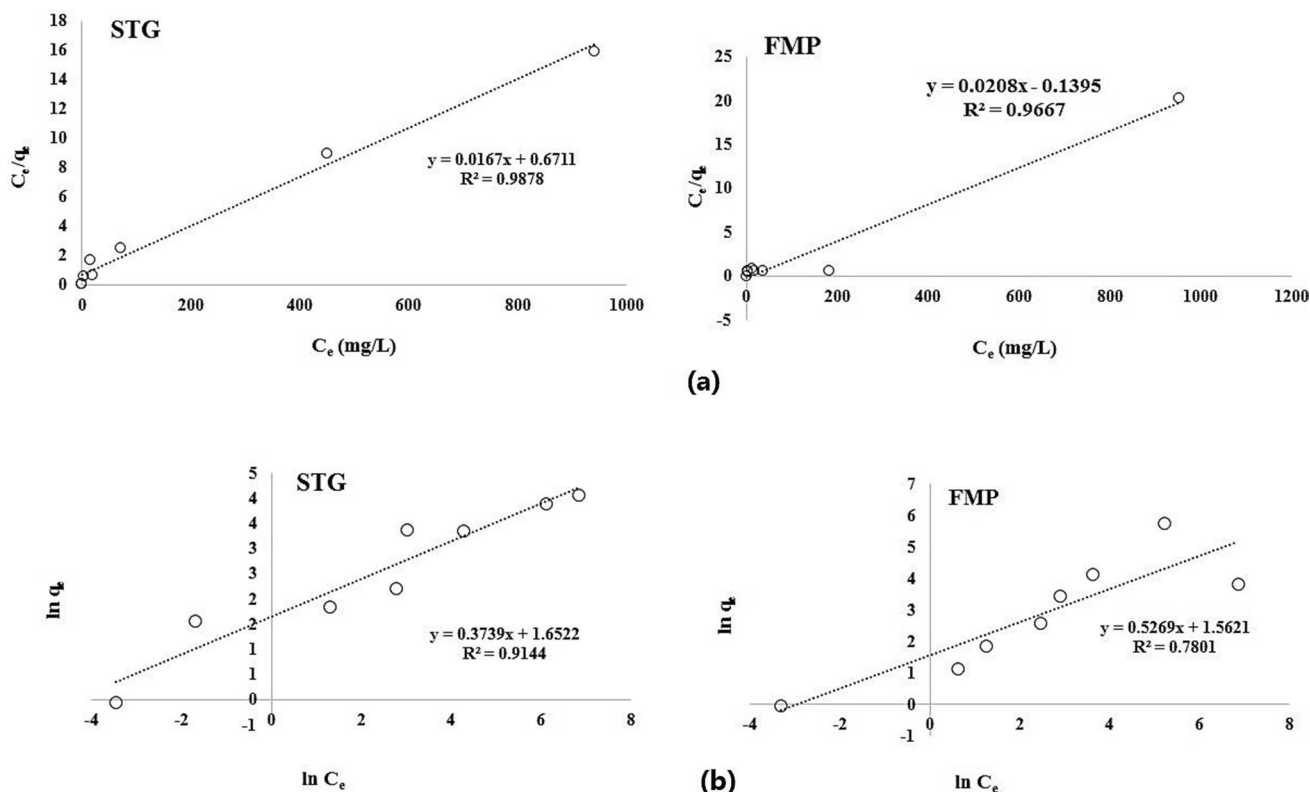


Fig. 11 a Langmuir and b Freundlich isotherms of STG and FMP by the magnetic kiwi peel

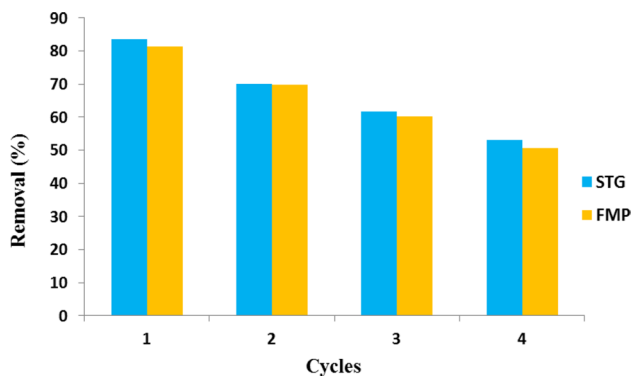


Fig. 12 Reusability of magnetic kiwi peel for removing STG and MP

where C_e and q_e displays the pollutant concentration at equilibrium (mg L^{-1}) and the amount of pollutant adsorbed (mg g^{-1}), respectively. The values of q_m (mg g^{-1}) and K_L (L/mg) reveal the maximum adsorption capacity and a Langmuir isotherm constant, respectively. The q_{max} and K_L values (Table 8) were determined from the slope and intercept of the linear plot of C_e/q_e versus C_e (Fig. 11a). As shown in Table 8, K_F (mg g^{-1}) and n denote the Freundlich

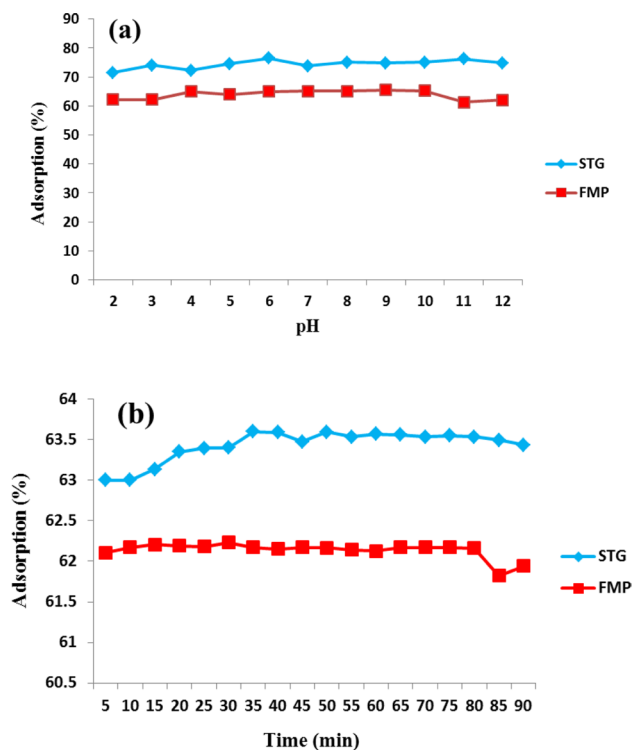


Fig. 13 The effect of pH and time on the stability of adsorbent

Table 9 The results obtained from real sample analysis

STG		
Batch 1		
Std	531.942	Removal (%)
Sample 1	194.496	63.43662
Sample 2	195.234	63.29788
Sample 3	194.927	63.35559
Mean		63.36336
Stdev		0.069694
RSD%		0.109991
Batch 2		
Std	535.038	Removal (%)
Sample 1	181.291	66.11624
Sample 2	181.247	66.12446
Sample 3	185.612	65.30863
Mean		65.84978
Stdev		0.468664
RSD%		0.711716
Batch 3		
Std	529.951	Removal (%)
Sample 1	192.374	63.69966
Sample 2	191.412	63.88119
Sample 3	191.679	63.83081
Mean		63.80389
Stdev		0.09371
RSD%		0.146871
FMP		
Batch 1		
Std	4732.74	Removal (%)
Sample 1	1750.195	63.01941
Sample 2	1748.916	63.04644
Sample 3	1761.239	62.78606
Mean		62.95064
Stdev		0.143167
RSD%		0.227427
Batch 2		
Std	4689.13	Removal (%)
Sample 1	1739.187	62.91024
Sample 2	1741.922	62.85191
Sample 3	1741.053	62.87045
Mean		62.87753
Stdev		0.029802
RSD%		0.047397
Batch 3		
Std	4758.01	Removal (%)
Sample 1	1749.321	63.23419
Sample 2	1748.728	63.24665
Sample 3	1748.495	63.25155
Mean		63.24413
Stdev		0.008951
RSD%		0.014153

constant and heterogeneity factor, respectively. These values were estimated from the linear plot of $\log q_e$ against $\log C_e$ (Fig. 11b). The values of n between 1 to 10 and $n < 1$

indicate favorable and unfavorable adsorption, respectively (Kaur et al. 2020). According to higher values of R^2 related to the Langmuir isotherm compared to the Freundlich, there is a monolayer distribution of STG and FMP on homogeneous active sites available on the magnetic adsorbent. The maximum adsorption capacity was obtained 59.88 and 58.08 mg g^{-1} for STG and FMP, respectively. The value of n equal to 2.67 for STG and 1.9 for FMP revealed the favorable adsorption.

Reusability of adsorbent

In order to decrease costs and waste production, the adsorbent recycling can be evaluated. The removal efficiency of adsorbent versus cycles (4 successive cycles) is illustrated in Fig. 12. It can be concluded that magnetic kiwi peel has high ability after four removal process (from 83.45 to 52.96%) for the reusability.

Stability of adsorbent

The effect of different pH (2–12) and time (5–90 min) was studied on the stability of the adsorbent. It can be seen that the adsorption changes are insignificant for both drugs (Fig. 13).

Real sample analysis

Sampling was done after producing 3 real batches. According to the obtained results (Table 9), the method has good precision and reproducibility for both drugs.

Comparison with literature

A comparison of the magnetic kiwi peel with previously reported adsorbents for the removal of various pharmaceutical pollutants was performed and given in Table 10. The removal efficiency and maximum adsorption capacity of the suggested adsorbent with a short adsorption time (35 min) were more satisfactory than other reported adsorbents.

Conclusion

In this study, the magnetic kiwi peel was synthesized and used to remove STG and FMP from an aqueous medium. HPLC technique was applied to calculate removal percentage values at different concentrations of drugs. The CCD experimental design was implemented to obtain the optimum conditions,

Table 10 Comparison of various adsorbent for the removal of different drugs

Adsorbent	Pollutant	q_{\max} (mg g ⁻¹)	Removal (%)	Time (min)	References
Artichoke leaves	MET ¹	30.3	–	45	Mahmoud et al. (2020)
Green synthesized Fe ₃ O ₄	DOX ²	98.04	73.6	1500	Weng et al. (2018)
Tea waste biochars	SMT ³	33.81	–	–	Rajapaksha et al. (2014)
Mung bean husk	RH ⁴	28.00	99.16	–	Mondal et al. (2015)
Banana peel biochars	CIP ⁵	21.00	–	<720	Pate et al. (2021)
Banana peel biochars	ACT	49.93	–	<720	Pate et al. (2021)
Magnetic kiwi peel	STG	59.88	73.59	35	This study
Magnetic kiwi peel	FMP	58.08	72.17	35	This study

¹Metformin²Doxorubicin³Sulfamethazine⁴Ranitidine hydrochloride⁵Ciprofloxacin⁶Acetaminophen

including pH, adsorbent dosage, and contact time for the highest peak area values of both pharmaceutical components. The R² values of adjusted determination and adequate precision demonstrated that the experimental data were matchable with the data predicted by the quadratic model. The pH, adsorbent dosage, contact time, the interaction of pH-adsorbent dosage, the interaction of pH-contact time, and the interaction of adsorbent dosage-contact time were considered the most efficient experimental factors for obtaining the peak area values for STG. On the other hand, the adsorbent dosage had a significant effect on the peak area values of FMP. The proposed adsorbent is simple, cost-effective, environmentally friendly, high efficiency, and reliable without needing a time-consuming synthesis process for the removal of pharmaceutical pollutants from aqueous solutions, which could be a suitable alternative to expensive and complex adsorbents.

Declarations

Conflict of interest The authors declare that they have no conflict of interest.

References

- Abbaszadeh S, Rashidi Nodeh H, Rafidah Wan Alwi S (2017) Bio-adsorbent derived from papaya peel waste and magnetic nanoparticles fabricated for lead determination. *Pure Appl Chem* 90:1
- Abolhasani S, Ahmadpour A, Rohani Bastami T, Yaqubzadeh A (2019) Facile synthesis of mesoporous carbon aerogel for the removal of ibuprofen from aqueous solution by central composite experimental design (CCD). *J Mol Liq* 281:261–268
- Achanti S, Rajeswari Katta R (2016) High-throughput liquid chromatography tandem mass spectrometry method for simultaneous determination of fampridine, paroxetine, and quinidine in rat plasma: application to in vivo perfusion study. *J Food Drug Anal* 24:866–875
- Akpomie KG, Conradie J (2020) Efficient synthesis of magnetic nanoparticle-Musa acuminata peel composite for the adsorption of anionic dye. *Arab J Chem* 13:7115–7131
- Almomani FA, Shawaqfeh M, Bhosale RR, Kumar A (2016) Removal of emerging pharmaceuticals from wastewater by ozone-based advanced oxidation processes. *Environ Prog Sustainable Energy* 35:982–995
- Angeles LF, Mullen RA, Huang IJ, Wilson C, Khunjar W, Sirotkin HI, McElroy AE, Aga DS (2020) Assessing pharmaceutical removal and reduction in toxicity provided by advanced wastewater treatment systems. *Environ Sci: Water Res Technol* 6:62
- Bankole DT, Oluyori AP, Inyinbor AA (2023) The removal of pharmaceutical pollutants from aqueous solution by Agro-waste. *Arab J Chem* 16:104699
- Baresel C, Harding M, Fang J (2019) Ultrafiltration/granulated active carbon-biofilter: efficient removal of a broad range of micropollutants. *Appl Sci* 9:710
- Bayuo J, Abdullai Abukari M, Bayetimani Pelig-Ba K (2020) Optimization using central composite design (CCD) of response surface methodology (RSM) for biosorption of hexavalent chromium from aqueous media. *Appl Water Sci* 10:135
- Bhattacharyya S, Das P, Datta S (2019) Removal of Ranitidine from Pharmaceutical Waste Water Using Activated Carbon (AC) Prepared from Waste Lemon Peel, Waste Water Recycling and Management. pp 123–141.
- Castro D, Rosas-Laverde NM, Aldás MB, Almeida-Naranjo CE, Guerrero VH, Pruna AI (2021) Chemical modification of agro-industrial waste-based bioadsorbents for enhanced removal of Zn (II) ions from aqueous solutions. *Materials* 14(9):2134
- Chang Lin C, Yen Lee C (2020) Adsorption of ciprofloxacin in water using Fe₃O₄ nanoparticles formed at low temperature and high reactant concentrations in a rotating packed bed with co-precipitation. *Mater Chem Phys* 240:122049
- Dhiman N, Sharma N (2019) Removal of pharmaceutical drugs from binary mixtures by use of ZnO nanoparticles. *Environ Technol Innov* 15:100392
- Elshafei AM, Othman AM, Elsayed MA, Al-Balakocy NG, Hassan MM (2021) Green synthesis of silver nanoparticles using *Aspergillus oryzae* NRRL447 exogenous proteins: optimization via central composite design, characterization and biological applications, environmental nanotechnology. *Monitoring & Management* 16:100553

- Farhadi SH, Sohrabi MR, Motiee F, Davallo M (2021) Organophosphorus diazinon pesticide removing from aqueous solution by zero-valent iron supported on biopolymer chitosan: Rsm optimization methodology. *J Polym Environ* 29:103–120
- Gomes D, Cardoso M, Martins RC, Quinta-Ferreira RM, Gando-Ferreira LM (2020) Removal of a mixture of pharmaceuticals sulfamethoxazole and diclofenac from water streams by a polyamide nanofiltration membrane. *Water Sci Technol* 81:732–743
- Gou X, Zhang P, Song Y, Qian F, Yu H, Zeng G (2017) Novel insights into the coagulation process for pharmaceutical wastewater treatment with fluorescence EEMs-PARAFAC. *Water Sci Technol* 76:3246–3257
- Gubitosa J, Rizzi V, Fini P, Nuzzo S, Cosma P (2022a) Regenerable kiwi peels as an adsorbent to remove and reuse the emerging pollutant propranolol from water. *Processes* 10:1417
- Gubitosa J, Rizzi V, Cignolo D, Fini P, Fanelli F, Cosma P (2022b) From agricultural wastes to a resource: kiwi Peels, as long-lasting, recyclable adsorbent, to remove emerging pollutants from water the case of ciprofloxacin removal. *Sustain Chem Pharmacy* 29:100749
- Gumieniczek A, Berecka A, Mroczek T, Wojtanowski K, Dabrowska K, Stepień K (2019) Determination of chemical stability of sitagliptin by LC-UV, LC-MS and FT-IR methods. *J Pharm Biomed Anal* 164:789–807
- Hermes N, Jewell KS, Falas P, Lutze HV, Wick A, Ternes TA (2020) Ozonation of sitagliptin: removal kinetics and elucidation of oxidative transformation products. *Environ Sci Technol* 54:10588–10598
- Jiang R, Tian J, Zheng H, Qi J, Sun S, Li X (2015) A novel magnetic adsorbent based on waste litchi peels for removing Pb(II) from aqueous solution. *J Environ Manage* 155:24–30
- Kalantary RR, Azari A, Esrafil A, Yaghmaeian K, Moradi M, Sharafi K (2016) The survey of Malathion removal using magnetic graphene oxide nanocomposite as a novel adsorbent: thermodynamics, isotherms, and kinetic study. *Desalin Water Treat* 57:28460–28473
- Kanakaraju D, Glass BD, Oelgemoller M (2018) Advanced oxidation process-mediated removal of pharmaceuticals from water: a review. *J Environ Manage* 219:189–207
- Kaur M, Kumari S, Sharma P (2020) Removal of Pb (II) from aqueous solution using nano-adsorbent of *Oryza sativa* husk: Isotherm, kinetic and thermodynamic studies. *Biotechnol Reports* 25:e00410
- Kit Loh GO, Yii Ling Wong E, Tze Fung Tan Y, Lin Lee Y, Hui Pang L, Chien Chin M, Damenthi N, Khiang Peh K (2020) Simple and rapid LC-MS/MS method for determination of sitagliptin in human plasma and application to bioequivalence study. *J Chromatogr B* 1159:122337
- Kooijman G, de Kreuk MK, Houtman C, Van Lier JB (2020) Perspectives of coagulation/flocculation for the removal of pharmaceuticals from domestic wastewater: a critical view at experimental procedures. *J Water Process Eng* 34:101161
- Krakko D, Illes A, Domjan A, Demeter A, Dobe S, Zaray G (2022) UV and (V)UV irradiation of sitagliptin in ultrapure water and WWTP effluent: Kinetics, transformation products and degradation pathway. *Chemosphere* 288:132393
- Kyzasa GZ, Deliyanni EA (2015) Modified activated carbons from potato peels as green environmental-friendly adsorbents for the treatment of pharmaceutical effluents. *Chem Eng Res Des* 97:135–144
- Liakos EV, Lazaridou M, Michailidou G, Koumentakou I, Lambropoulou DA, Bikiaris DN, Kyzas GZ (2021) Chitosan adsorbent derivatives for pharmaceuticals removal from effluents: a review. *Macromol* 1:130–154
- Liu M, Zhang X, Li Z, Qu L, Han R (2020) Fabrication of zirconium (IV)-loaded chitosan/Fe₃O₄/graphene oxide for efficient removal of alizarin red from aqueous solution. *Carbohydr Polym* 248:116792
- Mahmoud ME, Moneim El-Ghanam A, Saad SR, Mohamed HA, R, (2020) Promoted removal of metformin hydrochloride anti-diabetic drug from water by fabricated and modified nanobiochar from artichoke leaves. *Sustainable Chem Pharmacy* 18:100336
- Mallampati R, Xuanjun L, Adin A, Valiyaveetil S (2015) Fruit peels as efficient renewable adsorbents for removal of dissolved heavy metals and dyes from water. *ACS Sustainable Chemistry & Engineering* 3:1117–1124
- Mohd Zahri NA, Md Jamil SNA, Abdullah LC, Jia Huey S, Nourouzi Mobarekeh M, Mohd Rapeia NS, Shean Yaw TC (2021) Central composite design of heavy metal removal using polymer adsorbent. *J Appl Water Eng Res* 9(2):133–146
- Mondal S, Sinha K, Aikat K, Halder G (2015) Adsorption thermodynamics and kinetics of ranitidine hydrochloride onto superheated steam activated carbon derived from mung bean husk. *J Environ Chem Eng* 3:187–195
- Mrozik W, Stefanska J (2014) Adsorption and biodegradation of anti-diabetic pharmaceuticals in soils. *Chemosphere* 95:281–288
- Pashazadeh-Panahi P, Hasanzadeh M (2020) efficient removal of digoxin from aqueous solution using magnetic nanocomposite (Fe₃O₄-GO-SO₃H) as an advanced nano-adsorbent. *Nanocomposites* 6:66–75
- Pate M, Kumar R, Pittman C, Mohan D (2021) Ciprofloxacin and acetaminophen sorption onto banana peel biochars: environmental and process parameter influences. *Environ Res* 201:111218
- Pathak PD, Mandavgane SA, Kulkarni BD (2015) Fruit peel waste as a novel low-cost bio adsorbent. *Rev Chem Eng* 31:361–381
- Patil CS, Gunjal DB, Naik VM, Harale NS, Jagdale SD, Kadam AN, Patil PS, Kolekar GB, Gore AH (2019) Waste tea residue as a low cost adsorbent for removal of Hydralazine hydrochloride pharmaceutical pollutant from aqueous media: an environmental remediation. *J Clean Prod* 206:407–418
- Rajapaksha AU, Vithanage M, Zhang M, Ahmad M, Mohan D, Chang SX, Sik Ok Y (2014) Pyrolysis condition affected sulfamethazine sorption by tea waste biochars. *Biores Technol* 166:303–308
- Rani M, Shanker U (2018) Effective adsorption and enhanced degradation of various pesticides from aqueous solution by Prussian blue nanorods. *J Environ Chem Eng* 6:1512–1521
- Rao Amarachinta P, Sharma G, Samed N, Kumar Chettupalli A, Alle M, Kim JC (2021) Central composite design for the development of carvedilol-loaded transdermal ethosomal hydrogel for extended and enhanced anti-hypertensive effect. *J Nanobiotechnol* 19:100
- Sanz V, López-Hortas L, Torres MD, Domínguez H (2021) Trends in kiwifruit and byproducts valorization. *Trends Food Sci Technol* 107:401–414
- Sartape AS, Mandhare AM, Jadhav VV, Raut PD, Anuse MA, Kolekar SS (2017) Removal of malachite green dye from aqueous solution with adsorption technique using *Limonia acidissima* (wood apple) shell as low cost adsorbent. *Arab J Chem* 10:S3229–S3238
- Singh AK, Ketan K, Singh JK (2017) Simple and green fabrication of recyclable magnetic highly hydrophobic sorbents derived from waste orange peels for removal of oil and organic solvents from water surface. *J Environ Chem Eng* 5:5250–5259
- Suneetha A, Raja Rajeswari K (2016) A high throughput flow gradient LC-MS/MS method for simultaneous determination of fingolimod, fampridine and prednisone in rat plasma, application to in vivo perfusion study. *J Pharm Biomed Anal* 120:10–18
- Swarnalakshmi KS, Chinnaiyan P, Nivetha S, Nair AS (2018) Use of rice husk ash as an adsorbent to remove contaminants in water and

- comparison with advanced oxidation process – a study. *Materials Today: Proceedings* 5:24248–24257
- Weller D, Lörincz L, Sutter T, Reuter K, Linnebank M, Weller M, Zörner B, Filli L (2020) Fampridine-induced changes in walking kinetics are associated with clinical improvements in patients with multiple sclerosis. *J Neurol Sci* 416:116978
- Weng X, Ma L, Guo M, Su Y, Dharmarajan R, Chen Z (2018) Removal of doxorubicin hydrochloride using Fe_3O_4 nanoparticles synthesized by euphorbia cochinchinensis extract. *Chem Eng J* 353:482–489

Publisher's Note Springer Nature remains neutral with regard to jurisdictional claims in published maps and institutional affiliations.

Springer Nature or its licensor (e.g. a society or other partner) holds exclusive rights to this article under a publishing agreement with the author(s) or other rightsholder(s); author self-archiving of the accepted manuscript version of this article is solely governed by the terms of such publishing agreement and applicable law.